**Citation:** Bull, Jonathan M. and Scrutton, Roger A. (1992) Seismic reflection images of intraplate deformation, central Indian Ocean, and their tectonic significance *Journal of the Geological Society*, 149, (6), pp. 955-966.

# Seismic reflection images of intraplate deformation, central Indian Ocean, and their tectonic significance

J. M. BULL' & R. A. SCRUTTON[2]

[1]Department of Geology, University of Southampton, Highfield, Southampton S09 5NH, UK
[2]Department of Geology and Geophysics, The Grant Institute, University of Edinburgh, West Mains Road, Edinburgh EH9 3JW, UK

**Abstract: Multichannel seismic reflection profiles collected from the intraplate deformation area in the Central Indian Ocean Basin are used to describe brittle structures produced under compressive stress. Reflectors within oceanic basement are divided into four types: north-dipping and south-dipping reverse faults that are interpreted as reactivations of structures formed at the spreading-centre as outward and inward dipping faults respectively; lower-angle, north-dipping reflectors that probably represent new faults or faults just initiating; and sub-horizontal reflectors within the uppermost crust that are interpreted as hydrothermal alteration fronts. Within the sedimentary cover upwards fault propagation shows the faults steepening from c. 40° just above basement to near vertical and is preceded by sediment folding. A fractal analysis of faulting suggests two fault populations possibly reflecting different criteria for brittle failure. Measurements of north-south crustal shortening indicate a shortening rate of 2.5 (+ 0.9) mm $a^{-1}$, which is at the lower end of predictions from plate motions, but significant enough to recognize this area as a diffuse plate boundary. The formation of long-wavelength basement undulations and the reactivation of fracture zones and ridge-parallel fault fabrics are linked in a unified tectonic model driven by the high level of intraplate compressive stress in the area. There is little evidence from the seismic profiles for intraplate deformation starting before the widespread unconformity dated as 7 Ma.**

Plate motion models have until recently assumed that plate boundaries are well defined and that oceanic plates remain undeformed internally during their growth and destruction. Now there is good evidence that neither of these assumptions is necessarily true, with recognition of diffuse plate boundaries within the Indo-Australian and American plates (Gordon et al. 1990). The zone of intraplate deformation in the Central Indian Ocean (Fig. 1) is the best documented of these new tectonic elements. A variety of geophysical data sets reflect the compressive deformation: seismicity (Bergman & Solomon 1985; Petroy & Wiens 1989), geoid and gravity anomalies (Weissel & Haxby 1984; Stein et al. 1989), heat flow data (Stein & Weissel 1990), and seismic reflection profiles (Weissel et al. 1980; Neprochnov et al. 1988; Bull 1990; Bull & Scrutton 1990a). A recent ODP Leg (116) drilled through an unconformity separating pre- and syn-deformational sediments on the distal Bengal Fan dating the onset of deformation at 7Ma (Shipboard Scientific Party 1989). Although this unconformity is clear on all seismic reflection records from the area, an earlier unconformity is identified by Curray & Munasinghe (1989) in some places, which together with a new analysis of plate motions around the Indian Ocean triple junction by Royer & Chang (1991), raises the possibility of earlier compressional tectonics.

The status of the Central Indian Ocean as a zone of deformation was first noted from the large amount of intraplate seismicity (Sykes 1970). Thrust and strike-slip events at upper mantle depths on

E-W and N-S fault planes respectively (Bergman & Solomon 1985) testify to brittle failure of the core of the lithosphere. Maximum horizontal compressive stress vectors (Bergman & Solomon 1985; Cloetingh & Wortel 1986) imply sinistral transpression across the fracture zones through the area, which strike approximately 000-010°N. However, the intraplate deformation is perhaps most spectacularly revealed on seismic reflection profiles, on which it occurs at two spatial scales. A first order of deformation is represented by roughly ENE-WSW-trending, long-wavelength undulations of the oceanic basement and the overlying sedimentary cover. On seismic profiles and on satellite geoid and gravity maps (McAdoo & Sandwell 1985) wavelengths are seen to be 130-250 km with a mean of around 190-200 km. The amplitude of the undulations is 1-2 km. Geller et al. (1983) mapped the orientations of the undulation crests and troughs from seismic profiles which were then modified by Bull et al. (1992) as shown in Fig. 1. The offset of undulations across fracture zones was noted by Bull (1990) as being consistent with not only approximately N-S compression but also the strike-slip motion indicated by earthquakes.

Three models have been proposed to explain the undulations: uniform crustal folding (buckling) with the Moho paralleling basement (Weissel et al. 1980; McAdoo & Sandwell 1985); inverse boudinage with thickening beneath basement highs (Zuber 1987); and some form of block faulting (Neprochnov et al. 1988). Bull et al. (1992), using the results of analogue experiments, argued that buckling was the most likely mode of deformation. Seismic refraction studies carried out to detect the presence or absence of boudinage have been contradictory, with Leger & Louden (1990) supporting the crustal thickening model while Neprochnov et al. (1988) preferred uniform crustal folding. Interpretation of geoid and gravity anomalies is also ambiguous. Some authors argue for buckling (Haxby & Weissel 1986; Bull et al. 1992), others for inverse boudinage (Leger & Louden 1990).

Superimposed on the first order of deformation is a second order represented by faulted blocks 5-20 km in width bounded by approximately E-W (90-100°E, Fig. 11) reverse faults of Miocene and younger age which have throws of up to 600m (Weissel et al. 1980; Neprochnov et al. 1988). In basement these reverse faults dip at 35-45° and extend down to the expected level of the Moho (Bull & Scrutton 1990a). In the sedimentary cover they are steeper, dipping 40-90°. It is generally agreed that the faults are reactivations and propagations of the pre-existing oceanic basement fault fabric, but how motion on them relates to the motion displayed by earthquakes is not yet clear. Bull & Scrutton (1990a) suggested that compressional motion and shortening may have nucleated at upper mantle level and propagated through the crust by exploiting the pre-existing fault fabric.

An important indicator of the potential driving force behind any tectonic deformation is the surface heat flow pattern. Regionally, heat flow in the Central Indian Basin is normal, arguing against a deep thermal origin for the regional driving force. Indeed, the principal driving force for the deformation is thought to be a concentration of horizontal intraplate stresses arising from the style of the plate boundary forces (Cloetingh & Wortel 1986). Local heat flow highs occur, and have been modelled from ODP Leg 116 data as arising from active hydrothermal convection of fluids within fault zones, basement and adjacent sediments (Williams 1990). Although complimentary heat sinks have not been observed, it is assumed that relatively cold, sinking fluid must originate from the ocean via fault pathways or from enhanced dewatering of sediments under stress.

In this paper use is made of multichannel seismic reflection profiles collected on Charles Darwin Cruise 28 and some single channel reflection data (from the same cruise and from Lamont-Doherty Geological Observatory) to describe the character and development of the compressional structures in the crust in the Central Indian Ocean Basin. This is the first comprehensive interpretation of multichannel seismic (MCS) data from this setting. Close attentions paid to new images of faults extending throughout the deforming oceanic crust, to the nature of sub-basement reflectors,

accurate estimates of crustal shortening, as well as any evidence for deformation pre-dating 7 Ma, and to tectonic processes. The profiles collected by the Charles Darwin in 1987 comprise 12 fold coverage and are in part fully migrated (Fig. 2). These profiles improved the resolution of the sedimentary reflectors, removed multiples and better imaged near vertical fault traces in the sediments. A short piece of multichannel profile through the ODP Leg 116 sites has already been published (Bull & Scrutton 1990a, b). The area over which the study takes place is 0.0° to 5.5°S, 78.0°E to 82.0°E. Deformation is known to extend over a much larger area (Fig. 1), of which this study area is hopefully representative.

**Reflections from oceanic basement and crust**

Some of the most exciting observations on the multichannel seismic data are four types of intra-basement reflector, three with significant dip (> 20") and a fourth with low dip showing strong, sub-horizontal character in the top of basement. The four types are classified according to their direction and amount of dip and the degree of offset in the basement/cover interface: (i) north-dipping events which offset the basement/cover interface; (ii) rare south-dipping events which also offset the basement/over interface; (iii) north dipping, slightly lower-angle events that do not offset the basement/cover interface; (iv) sub-horizontal reflectors that also do not offset the basement/cover interface. Types (i) and (ii) will be referred to as north- and south-dipping basement faults respectively. The third type could be either small offset fractures or compositional boundaries and will henceforth be referred to as north-dipping basement reflectors.

*(i) North-dipping basement faults.* This is the most common type of intra-basement reflector. In the vast majority of cases the basement/cover interface is offset in a reverse sense with characteristic hanging-wall anticlines in the overlying cover. There is no clear example of a normal offset in our data. Fully migrated multichannel seismic profiles (Fig. 3) show typical examples of these north-dipping reverse faults.

Figure 3 shows many prominent north-dipping faults in basement which can be correlated with more steeply dipping faults in the sedimentary cover. The dip of the faults in basement ranges from 30-40° in this example, with a rapid increase in dip to > 65° in the sedimentary cover. Faults extend down to around 10s TWT (two-way time), which is approximately Moho depth, but the Moho itself is not imaged. The curvature of the fault planes in basement may be a function of velocity increasing with depth. Following depth conversion on a selected panel of data the faults appear to be planar. In the uppermost oceanic crust resolution of the faults is lost, possibly because of an increase in dip, or because of an increase in fracturing or the presence of surrounding rough topography.

On this section there is some evidence for a decollement within the oceanic crust as indicated by the dashed line with a dip of 17-18°. Note that the tip of the decollement is just starting to flex the basement/over interface as though it is a propagating structure. The structure is essentially a blind thrust and the flexing of the basement surface is effectively a fault propagation fold as described by Chester & Chester (1990).

To the right of the section there is evidence for fault crosscutting relationships. Also marked are examples of possible hydrothermal alteration fronts. Both of these will be discussed later.

As demonstrated by Bull (1990), the spacing of faults throughout is irregular. Throws also vary, and large amplitude displacements on north-dipping reverse faults can occur as isolated examples (Fig. 4). Characteristic features are present here, with a hanging-wall anticline, a fault plane dip in basement of 37" and very large (c. 600 m) reverse offset of the basement/cover interface. The fault is not resolved for the first 0.5 S below basement and then is imaged down to 8.6 S TWT.

*(ii) South-dipping basement faults.* The imaging of this type of reflector is much rarer within the survey area and where the faults are resolved they are substantially less clear. In a similar manner to the north-dipping faults, the basement/cover interface is offset in a reverse sense and faulting extends into the cover with the creation of hanging-wall anticlines.

Within the survey area the clearest example of a south-dipping fault is illustrated in Fig. 5. The basement reflector is offset in a reverse sense. While the fault is clearly resolved between 9.0 and 10.1 S, it is poorly resolved in basement between 8.0 and 9.0 S, perhaps because of the large amount of multiple energy present in this part of the section. Because this section was not migrated it is difficult to estimate true fault dip. However, by comparison with other migrated faults, the fault is likely to have a dip between 35 and 40°. More generally, the faults of this group appear to have dips of c. 40-45°, a few degrees more than the north-dipping faults. Furthermore, in comparison with the basement/over offset for the north-dipping faults, the offset, while remaining reverse, appears to be more vertical for this group.

An extended length of migrated profile (Fig. 6) illustrates a series of south-dipping but, typically poorly imaged reverse faults. In this section spacing and amplitude of the faults appears to be quasi-regular, but this is certainly not the case over most of the deformation area.

The conclusion from single-channel seismic data (Bull 1990) that the complex fault pattern is the result of the reactivation of two sets of original spreading-centre normal faults, inward and outward facing, has clear implications for the multichannel observations. Faults dipping at 30° towards the north represent reactivated spreading-centre formed outward-dipping normal faults while faults dipping at 40-45°+ towards the south are reactivated original inward-dipping normal faults. Deformation in the sedimentary cover suggests that the two sets occur with approximately equal numbers. Thus, resolution in basement of far more of the outward-dipping faults, and their greater clarity relative to the inward-dipping set, could be because of their lower dip. This is consistent with the observation of generally steeper reverse offset of the basement/over interface for the inward-dipping faults.

*(iii) North-dipping basement reflectors.* Even in areas where there is little tectonic deformation there are regularly spaced north-dipping, strong, sub-basement reflectors that do not intersect basement. These reflectors (Fig. 7) typically start 0.4-0.5s TWT beneath the top of basement and continue to 1.0 s. With dips of 20-30° (estimated from migrated and stacked sections) they generally have lower dip than the north-dipping basement faults.

There would seem to be two possible interpretations of north-dipping reflectors which do not offset the basement/over interface. Either they are original outward-dipping normal faults on which reactivation is just initiating, or they are some form of compositional boundary within the crust, such as the relict top of the spreading-centre magma chamber. Their regular spacing (5-6 km in Fig. 7) is consistent with both of these hypotheses. However, the observation of the flexure in the top of basement in close proximity to some of the dipping reflectors, suggesting fault reactivation, and their similar reflection character to fully developed faults (transparent in the uppermost crust) strongly supports the view that they are original spreading-centre formed outward-dipping normal faults. Estimation of average dip from a mixture of migrated and unmigrated profiles is difficult, although the difference between 20-30° and 30-40° between the low offset faults and their fully reactivated counterparts is likely to be real. If the difference is real then it suggests that either originally steeper dipping outward-dipping faults are reactivated preferentially or steepening occurs with reactivation. Fault block rotation can easily be estimated to be a maximum of 5" rather than the 10" required to explain the difference in dip between the two types.

*(iv) Sub-horizontal basement reflectors.* Where the quality of the multichannel profiles is particularly high (e.g. Fig. 3a and b) sub-horizontal basement reflections are observed within 0.3-0.7 S TWT of the top of oceanic basement. The strong reflectors are usually undulatory and often truncate against either north or south-dipping reverse faults. Illustrated in Fig. 3 is an example, with the depth to the basement reflector from the top of oceanic layer 2 varying from 0.35 to 0.7 S TWT. This reflector has a geometry dissimilar to any of the overlying strata, thus removing any possibility that it represents a multiple. It appears to be truncated at one end by faulting. There are two possible explanations for the sub-horizontal basement reflections: either the magmatic boundaries between the dykes and gabbros (McCarthy et al. 1988), or subsequently imposed hydrothermal alteration fronts (White et al. 1990). Hydrothermal circulation along fault planes has been proposed to explain the non-linear temperature gradient recorded down one of the ODP Leg 116 Holes (Shipboard Scientific Party 1989) and to explain the localized high heat-flow in the intraplate area (Geller et al. 1983). Hydrothermal circulation is known to penetrate 1-3 km into the crust at spreading-centres and to result in a thin transition zone between unaltered and hydrothermally altered layers (Campbell et al. 1988). The observation of fault planes truncating the sub-horizontal reflectors, the depth of the reflectors (< 2 km beneath basement), and the presence of vigorous hydrothermal circulation

**Discussion**

Comparison of the features described here may be made with reflectors imaged in the crust in the Western North Atlantic (Fig. 4; White et al. 1990). White et al. (1990) divide images obtained into several classes depending on whether they occurred on ridge-parallel or ridge-perpendicular profiles and on the nature of the reflectors. For the dipping reflectors White et al. (1990) conclude that they have imaged two different structures, one striking parallel to the ridge crest and dipping 30-40° towards it and the other dipping 20-30° parallel to the ridge. All the whole crustal reflectors imaged on ridge-perpendicular profiles are interpreted as inward-facing normal faults originally formed at the spreading-centre with fracturing, hydrothermal alteration, and steepening of the faults in the upper crust cited as reasons for imaging of some of the faults only in the lower crust. They also speculate that some of the lower crustal reflectors may have magmatic origin. The shallower dipping reflectors imaged on the ridge parallel profiles are interpreted as later compressional failures, generated by thermo-elastic stresses as the oceanic lithosphere cools.

In comparison with the Darwin Indian Ocean profiles, the dominant fault set that is imaged is the inward-dipping set as opposed to the outward-dipping set. It should be noted, and this was not stressed by White et al. (1990), that a third of the lower crustal dipping reflectors on ridge-perpendicular profiles were dipping away from the spreading-centre and could be interpreted as original outward-dipping normal faults. These possible outward-dipping faults have lower dip than the inward-dipping faults, which is consistent with the observations from the Indian Ocean. In general, the fault sets in the Atlantic Ocean crust have lower dips than those imaged in the Indian Ocean crust.

Although the Darwin multichannel profiles usually only reveal the outward-dipping faults below basement level, statistical analysis of the fault sets on all the seismic profiles available suggests that approximately equal numbers of inward and outward-dipping faults have been reactivated (Bull 1990). In the Atlantic two-thirds of the faults imaged appear to be inward-dipping. This difference, although the database is small, can be interpreted as being due to differing acquisition systems, preferential reactivation of one set in the Indian Ocean or differing spreading rate. The spreading rate that formed the Atlantic crust (c. 20mm $a^{-1}$) is approximately three times slower than that which formed the Indian crust (c. 60 mm $a^{-1}$).

Comparison may also be made of the Indian Ocean fault geometry with that documented by contemporary seismicity at present day spreading centres. Huang & Solomon (1988) found that large earthquakes along the axes of slow spreading mid-ocean ridges have mechanisms indicating normal faulting on planes dipping at 40-55°. This is broadly consistent with the dips of faults observed in the Central Indian Ocean Basin of 30-45°+. Huang & Solomon (1988) suggest that much of the fault activity is likely to be concentrated on inward-dipping faults given that the topographic relief of the median valleys of slow-spreading ridges is dominantly formed by this fault set (Macdonald & Luyendyk 1977). Additionally seismic moments and source durations at active spreading centres are found to be consistent with typical fault lengths of 10 km, comparable or slightly longer than the mean length of reactivated faults in the intraplate deformation area (Bull 1990).

However, while Huang & Solomon's (1988) study is useful for crude comparison with observations in the Central Indian Ocean Basin, their work was on slow-spreading ridges. Little analogous work has been carried out on fast spreading ridges (barring the study of Riedesal et al. (1982) discussed below) similar to the one that produced the Central Indian Ocean Basin lithosphere. Earthquake seismology studies along mid-ocean ridges are particularly useful in determining the depth extent of faulting and hence giving important information on the depth to the brittle-ductile transition in the axial region. Using the assumption that the centroid depth marks the man depth of fault slip, it appears that faulting, for half spreading-rates of 20mm a-' or less, extends from 2 km to 10 km beneath the seafloor, into the upper mantle, with the greatest centroid depths shallowing with increasing rate (Fig. 3; Huang & Solomon 1988). They show that for half spreading rates of 25mm a-' the brittle layer may be as little as 3 km thick. By extrapolation to fast spreading ridges, the thickness of the brittle layer would be expected to decrease further. One local study (Riedesal et al. 1982) of microseismicity on the East Pacific Rise at 21°N, where the half spreading-rate is 36mm a° (MacDonald & Luyendyk 1985), concluded that fast-spreading ridges are characterized by only small magnitude earthquakes, and that the brittle layer is only 2-3 km thick.

From these studies it is possible to conclude that for the half spreading-rate that formed the Central Indian Ocean lithosphere (c. 60mm a-') the thickness of brittle deformation would have been only a few kilometres. Faulting to the depth presently observed would have been unlikely at the original spreading-centre. Therefore, the deepest portions of the faults imaged on the multichannel profiles, which extend to lower crustal and possible mantle depths, may not have originated at the spreading centre.

**Structures in the sedimentary cover**

*Reflection character*

Quite a large database of single channel seismic reflection profiles is now available for this area of intraplate deformation. From this, the salient, general features of the gentle anticlinal folds and high-angle reverse faults in the sedimentary cover are known (Weissel et al. 1980; Neprochnov et al. 1988; Bull 1990). The large database has allowed a statistical analysis of over 250 faults to be carried out by Bull (1990), who identified equal numbers of north-throwing and south-throwing displacements, whilst on a local scale, in the vicinity of the Leg 116 ODP sites, detailed structural mapping of two fault blocks has revealed a 'twisting' process during fault reactivation (Shipboard Scientific Party 1989). In this study, the processed multichannel seismic data, in some cases migrated, provides a much clearer image of individual faults and folds. The extent to which features seen on the multichanne1 seismic data are typical of the whole area of study can be assessed by reference back to lower quality single channel profiles. It is convenient to present the new

observations on folds before those on faults because it is clear that folding precedes brittle failure as structures develop.

(i) Folds. Open anticlinal folds of 5-10 km wavelength are widespread in the sedimentary cover. Some are without any observable associated faulting, but more commonly they occur with limited faulting in the deeper parts of the succession or with faulting extending throughout the succession from basement to sea floor or close to the sea floor. Since the resolution of the seismic data is probably 20-25m it is possible that displacement on a fault or faults of up to this amount accompanies all folds without it being noticeable. The anticlines become hanging wall features when faulting occurs, and are sometimes paired with lower amplitude foot-wall synclines. The general shape of the folds is closely related to the movement of the basement surface, with a steep limb developing above the fault scarp growing in basement. These steep limbs dip at up to 15-20' in the presence of faults and up to 10" where failure has yet to occur. Sometimes the underlying hanging wall basement surface appears to be involved in the folding, but this must be distinguished from original basement topography associated with the fault formed at the spreading centre and from the effect of many small antithetic faults down-throwing into the major fault zone.

A feature of the folding is that higher in the succession it is of lower amplitude and longer wavelength, i.e. more open. With velocities increasing with depth this feature is probably even more pronounced than it appears on the migrated time sections (e.g. some of the folds in Fig. 3). The most likely cause of this is the upwards attenuation of the structure from an abrupt displacement of basement via the sediment column in which some internal, elastic-plastic deformation is occurring in order to accommodate the displacement. When faulting of the steep limb of the fold takes place elastic rebound of the fold might be expected, but this does not seem to be enough to correct for the initial folding effect.

Where faults are absent or near vertical, the folds must be the principal means of shortening in the sedimentary cover. Thus the tighter folds at depth should provide the same shortening as the more open, longer wavelength folds at shallower levels. This mode of shortening is modified as faulting propagates through the fold, and is mentioned below in the section on faults.

The growth of the fold structures is recorded in the sediment onlap patterns on the shallower dipping limb that overlies the tilted basement surface of the fault block. Although it is difficult to correlate across faults it does appear, and is generally agreed (Curray & Munasinghe 1989; Shipboard Scientific Party 1989), that fold growth and onlap started throughout this part of the deformation area at the same time, 7 Ma ago. On most seismic reflection profiles the unconformity and onlap representing the onset of deformation are recognizable. In some places two or even three or more onlap patterns can be identified above this unconformity. In the ODP drilling area the multichannel seismic profile clearly shows four major onlap episodes (Fig. 8) with the possibility of several more below the level of seismic resolution. The Shipboard Scientific Party felt that the structures had developed gradually from 7 Ma. This seems likely, there being repeated shortening events for individual fault blocks which accumulated to produce regional shortening. Assuming that this episodic shortening is regional, it has important implications for whether or not the present day tectonic activity, reflected in seismicity for example, is typical of the intraplate deformation through time. An inspection of the sedimentary succession has been made at deeper levels for any evidence of fold growth prior to 7 Ma. An Eocene unconformity has been recognized by Curray & Moore (1974) and plate reconstructions around the Indian Ocean triple junction suggest some shortening across the area of deformation as early as 25 Ma ago (Royer & Chang 1991). There is no convincing evidence for any earlier onlap patterns, however, although small features, below seismic resolution, cannot be ruled out.

(ii) Faults. Virtually all the faults observed are high-angle reverse faults. Along strike they reach up to 40 km in length but have a mean length of less than 10 km. Throws are up to 600 m. About equal numbers throw to the north as to the south, with the north-throwing one slightly wider spaced, on average 11 km apart as opposed to 8 km mean separation for south-throwing ones. Spectacular 'cascades' of faults at regular spacing are observed in a few places (Fig. 6). A few steep normal faults are observed. Notable amongst these are small faults in the cover over the Indrani Fracture Zone at 2.9°S 79.1° E and faults that are concave towards the hanging wall so that they change from reverse at depth to normal at shallower levels.

A common feature of the faults is a change in dip from as little as 20° just above basement to sub-vertical higher in the succession. The steepening of the fault plane proceeds rapidly so that dips in excess of 65° are reached a few hundred metres above basement. Such dramatic steepening may result from the stress drop associated with the change in rheology from oceanic basement to the thick sedimentary cover. In addition, a component of strike slip motion during reactivation may be responsible, since laboratory studies of reactivation by Richard & Krantz (1991) indicate that strike-slip facilitates fault steepening. Features typical of strike-slip faulting, such as anastomosing fault planes, flower structures and alternating fault throws with depth, have not been seen.

On several faults across which it is possible to confidently correlate reflectors it can be shown that displacement decreases steadily upwards. The loss of displacement is initially surprising because any faulting occurring since the onset of deformation should have displaced all pre-7 Ma formations by an equal amount, there being no convincing evidence from onlap patterns for pre-7 Ma deformation. However, if the faults grow by upwards propagation, as has been previously suggested, displacements would be more advanced at depth. There are other faults which do appear to have a roughly constant offset throughout the pre-7Ma succession, and these probably formed rapidly at the onset of deformation or at one specific time thereafter or are faults on which propagation is complete. The fact that numerous faults have completed their formation at an early stage is illustrated in Fig. 6 where up to 500m of undisturbed sediment has accumulated in an undulation trough. An interesting pair of faults is illustrated in Fig. 9. The south fault displays the common pattern of fault displacement decreasing upwards. Within basement it appears to displace and hence post-date the north fault. The north fault records displacement that is approximately the same throughout the pre-7 Ma succession. The latter is interpreted to have resulted from a single, rapid phase of movement or complete propagation, while the south fault is younger and still growing. In general, high-angle reverse faults have been shown to propagate a great distance relative to their offset and show only weak associated folding (Chester & Chester 1990), and that is what is observed here.

The shortening potential of the high-angle reverse faults is small, but greater near to basement where their dip is lower. Simple geometrical calculations show that a consistent percentage shortening is obtainable on relatively tight folds with some reverse faulting in the steep limb and on more open, longer wavelength folds at a shallower level.

**Discussion**

There is very little documentation of the style and development of high-angle reverse faults in sedimentary cover arising from the generation or reactivation of moderately dipping faults in basement. The Indian Ocean faults provide a rare example of this type of deformation. Low angle thrusts in orogenic thrust-fold belts commonly steepen upwards, and are the result of crustal shortening, like the structures discussed here, although they are not necessarily the result of the reactivation of pre-existing basement faults. On the other hand, movement of basement along

vertical faults, which has been examined both in the laboratory (Lowell 1970) and in the field (Prucha et al. 1965), tends to produce faults that flatten as they propagate upwards through the cover with shortening occurring only as a local feature. The inversion of basement involved normal faults in sedimentary basins has been studied (Koopman et al. 1987), but with little indication that new, upward-steepening reverse faults of the Indian Ocean type are produced. From these previous studies it seems that two types of steep reverse cover faults may be recognized: those that arise from crustal shortening and steepen upwards, and those that arise from vertical movements in basement and flatten upwards. The faults in the Indian Ocean are examples of the former.

A set of analogue laboratory experiments that quite closely reproduces the structural style seen here was conducted by Richard & Krantz (1991). On a basement fault of dip 54° with a cover of 'brittle' sedimentary rocks reverse motion produced two faults propagating through the cover, one a co-linear prolongation of the basement fault, the other a gently steepening fault originating from the same basement displacement. The main objective of the experiments was to observe the effect of strike-slip motion, however. With subsequent strike-slip on the basement fault more faults displaying strong steepening, and even overturning, were produced. Although the Indian Ocean examples have only one fault plane (plus, perhaps, small ones below the level of seismic resolution), that fault plane has the characteristics of those produced by strike-slip in the experiments. Thus, there is a strong suggestion that some strike-slip motion is associated with the reactivation of basement blocks in the Indian Ocean. The observation and discussion presented here consider only the two-dimensional character of the folds and faults, yet each fold and/or fault structure, is on average less than 10 km long. In the vicinity of the ODP Leg 116 sites the along-strike variation in fold development and fault throw is quite dramatically demonstrated, with 'twisting' of fault blocks, presumably about a horizontal axis, invoked to explain it. The limited length of the faults appears to be a direct inheritance from the oceanic basement fabric. Deformation has not progressed far enough, as yet, to encourage individual faults to link up. More advanced stages of deformation may lead to this.

**Tectonic processes**

*Fractal analysis: two modes of faulting?*

The second spatial scale of deformation, folds and high-angle reverse faults, appears to contain two different fault populations, probably representing the original ridge-parallel inward and outward-facing fault sets (Bull 1990). Here, we expand on this study of fault spacing, and look at fault amplitude using frequency distributions. In recent years many geological and geophysical phenomena have been investigated for power-law relationships, and have been found to satisfy the relation $N \propto r^{-D}$ where N is the number of objects with a characteristic size greater than r. Phenomena which have been found to follow a power-law relationship include earthquake magnitudes, ore deposits, size of oil-fields and the size of islands. Recently Walsh et al. (1991) in a comprehensive study of the Troll oilfield (North Sea) found a single power-law relationship between fault displacements and fault density over six orders of magnitude of fault displacement. The Central Indian Ocean Basin is an excellent area in which to test power-law relationships in structural geology. The study area, of originally simple structure, has been subjected to later deformation with the reactivation of faults with a single orientation (c. 100° E).

The dataset comprises 271 fault spacings recorded on single and multichannel seismic profiles orientated in a N-S direction. One major deficiency with the dataset is that there is little control on the along strike continuity of faults except to say that, in general, they have a length of < 10 km. Therefore in the discussion that follows sampling is only adequate in a two-dimensional sense, albeit

in an orientation roughly perpendicular to the structural strike. For fault amplitude only data from multichannel profiles (61 faults) is included, where there is excellent resolution of the basement offset, and hence control on fault amplitude. All measurements have been made with respect to the faulted basement/cover interface. Fault amplitude has been converted from the vertical two-way time (in seconds) offset across this interface to metres by assuming a velocity of 3000 m $s^{-1}$ for the lowermost sediment package.

The cumulative frequency plot for fault amplitude (Fig. 10a) seems to suggest two different power-law distributions. One distribution for faults less than 150 m (0.1 S TWT) has a D value of c. 0.6 and another distribution for faults greater than 150m has a D value of 1.9.

The first question to resolve is whether the sharp change in slope is due to incomplete sampling. Sampling is certainly adequate for all faults down to 0.03 s displacement, and thus the change in slope is unlikely to be due to resolution. Another reason for the change in slope could be related to under-sampling in 3D of the smaller faults. As discussed above, this is not a problem, especially as this would tend to produce a more gradual roll-over rather than the sharp kink in the graph.

We suggest that the change in distributions may be related either to the thickness of the strong brittle layer, or to there being two families of faults. For the first hypothesis, one set of faults (smaller values of fault amplitude) maintains a distribution corresponding to failure within the strong brittle layer, and the other distribution (larger values of fault amplitude) maintains a distribution corresponding to faults that have penetrated throughout the brittle upper layer of the oceanic lithosphere. One possible mechanism for the formation of these two fault populations is that the whole brittle layer set have developed by propagation upwards from the brittle/ductile transition (see later discussion); while the 'intra' strong layer population have resulted from relatively lower stresses within the upper brittle lithosphere. Alternatively one of the fault distributions may result from reactivation of the pre-existing fabric, while the other set may represent the initiation of new faults.

The cumulative frequency distribution for fault spacing (Fig. 10b) does not follow any obvious power-law distribution with the gradient apparently changing uniformly over all values of fault spacing.

*Estimates of shortening from multichannel seismic reflection profiles*

The multichannel profiles can be used to make an estimate of the amount of shortening caused by the intraplate deformation. With knowledge of the spatial extent of the deformation and the timespan of activity an estimate of the average rate of shortening can be obtained.

As already discussed, the tectonic deformation can be divided into two spatial scales represented by the long wavelength undulations and short wavelength folds with reverse faults. It has previously been recognized that the long wavelength undulations contribute little to the total shortening within the deformation area (Weissel & Geller 1981; Gordon et al. 1990). By coarse digitization of oceanic basement from seismic profiles and depth conversion using the velocities from Bull & Scrutton (1990b) we found that the long wavelength undulations had certainly contributed much less than 0.1% shortening, in agreement with the previous studies.

Previous estimates of shortening due to reverse faulting have been hampered by relatively poor quality of single-channel seismic profiles available (Weissel & Geller 1981). The multichannel profiles facilitate a better estimate, and using a method very similar to that of Weissel & Geller (1981) on both migrated and depth-converted sections we have tried to deduce the average horizontal

shortening due to reverse faulting. We estimate shortening to be 1.2 (± 0.4 )%. For the approximate 1500 km north-south extent of the deformation this corresponds to a total shortening of 18 (± 6) km. If deformation is assumed to have started at 7 Ma and to have been steady to the present, this implies a shortening rate of 2.5 (± 0.9) mm $a^{-1}$. This rate is towards the lower end of plate motion predictions (Gordon et al. 1990), but rather more than a previous estimate made from single channel profiles of c. 1 mm $a^{-1}$. The pattern of deformation on the seismic profiles suggests that there was a major shortening event at 7Ma and several smaller pulses since then, so higher rates probably would have pertained at times.

*Tectonic history*

The main tectonic elements described in this paper can be incorporated into a single coherent model of strain in the Central Indian Ocean Basin. It seems certain that intraplate compressive stress orientated NNW-SSE was responsible for the long wavelength undulations striking WSW-ENE and for the sinistral reactivation of the fracture zones that trend 000-010°N through the deformation area (Fig. 1). The stress field generated between fracture zones in this case would in turn encourage the development of Riedel shears between fracture zones, the conjugate element of which is approximately parallel to the reverse faults developed by structural reactivation in the basement (Fig. 11). Indirect evidence for a component of strike-slip motion on the reverse faults is consistent with this model, which predicts that the motion would be dextral. The present structural style suggests no more than a limited development of this model so far, but we may predict that in the future structures will develop along the same lines provided the principal compressive stress direction remains NNW-SSE.

The model proposed above explains the overall relationship between the main structural elements in planform. It does not address the mechanics of the fault/undulation relationship in cross-section. This is certainly not fully understood at present, with answers needed to such questions as whether any faulting by reactivation preceded buckling and the formation of the undulations or vice versa. A detailed stratigraphic analysis of the seismic data might reveal the relative timing of events but the problems of correlation along and between seismic profiles must be overcome.

We argued in a previous paper (Bull & Scrutton 1990a) that brittle deformation nucleates at the brittle/ductile transition in the lithosphere and propagates upwards reactivating the ridge-parallel fabric in the crust. We now suggest that a minor amount of dextral slip accompanies this propagation. There is limited evidence from our multichannel profiles for decollements in the lower crust being involved in this process, but conclusive evidence is required by further investigation using improved MCS systems. What is clear is that when the brittle deformation reaches the upper parts of the crust it progresses upwards using fault propagation folds. These folds deform the basement-sedimentary cover interface and the cover itself before faulted offset of the basement-cover interface occurs. With basement offset the folds develop a steep limb and propagate further upwards through the cover, becoming more 'open' higher up. As faulting propagates 'behind' the folding so the process of limb steepening and eventual failure passes up through the succession. Generally it is clear from sediment onlap patterns that the tectonic history of the folds and faults is complex with many events after the initial onset of deformation. In places, it is clear that some faults have formed quickly. It is likely that these major single events occurred at the onset of deformation.

Within this part of the Central Indian Ocean Basin we find no evidence for the Eocene unconformity described by Curray & Moore (1974) and Curray & Munasinghe (1989) over the Ninetyeast Ridge and within the thick sedimentary sections of the Bengal Fan. Indeed, there is no significant evidence for intraplate deformation prior to the 7 Ma unconformity dated by the ODP Leg 116, although some

faults that terminate half way up the sedimentary succession might be early deformation structures rather than young propagating structures. Reasons for the timing of the onset of deformation at 7Ma are still poorly known although in general the shape of the plate boundary configuration is thought to be responsible for the high compressive stress levels.

**Figure Captions**

Fig. 1. Tectonic fabric in the Central Indian Ocean Basin showing the location of basement undulation crests (+ +) and troughs (-) from Geller et al. (1983) modified by Bull et al. (1991), major fracture zones (F) from Royer et al. (1991), and the limit of the Bengal Fan (dotted line). Isobaths in kilometres. The inset shows the location of the main map with respect to plate boundaries. A diffuse plate boundary (stipple) separates the Indian and Australian plates (after Stein et al. 1989). In the bottom left corner a stress ellipse shows the relationship between intraplate stress direction, fracture zones on which sinistral focal mechanisms occur (Bergman & Solomon 1985) and undulations. Undulations are often discontinuous across fracture zones.

Fig. 2. The location of seismic profiles used in this study. Apart from the Charles Darwin Cruise 28 profiles (CD28), all profiles are from Lamont-Doherty Geological Observatory (LDGO). SCS, single channel seismics; MCS, multichannel seismic. Also shown are the locations of sections of profile illustrated in other figures.

Fig. 3. Uninterpreted (top) and interpreted (bottom) stacked and migrated multichannel profile through the ODP Leg 116 Sites (for position see Fig. 2). Clearly seen are north-dipping reverse faults that extend down to approximately 10 s TWT. On this profile there is limited evidence for a decollement which is propagating towards the south as a blind thrust with a fault propagation fold developing at its tip. Also shown are sub-horizontal basement reflectors within the top of basement that frequently truncate against fault planes. These are interpreted as hydrothermal alteration fronts.

Fig. 4. A section of fully processed and migrated multichannel profile whose position is shown in Fig. 2, illustrating an isolated large north-dipping reverse fault, folding and associated minor faulting. The north-dipping reverse fault has a dip of 37° in basement and is interpreted as a reactivated spreading-centre formed outward-dipping normal fault. Note the complex fault planes in the sedimentary cover.

Fig. 5. A section of fully processed multichannel profile whose position is shown in Fig. 2, which is interpreted as a reactivated spreading-centre formed inward-dipping normal fault. The fault plane in basement is likely to have a dip between 35 and 40°.

Fig. 6. A section of uninterpreted (top) and interpreted (bottom) fully processed and migrated multichannel profile whose position is shown in Fig. 2. Towards the northern end of the profile is a basement high representing the prominent crest of an undulation while the central portion shows part of a well-developed trough. A 'cascade' of south-dipping reverse faulting can be seen. Note that in the lower parts of the sections a large amount of noise is present.

Fig. 7. A section of fully processed multichannel profile whose position is shown in Fig. 2 illustrating regular north-dipping reflectors that do not offset the basement/over interface. These are interpreted as unreactivated spreading-centre formed outward-dipping faults. (Fig. 2).

Fig. 8. Line drawing of part of the multichannel profile illustrated in Fig. 3 through the fault block containing ODP Sites 717 and 719. This shows that onlap patterns within the sedimentary over are not uniformly developed as would be expected for gradual and uniform fault motion since the onset of deformation. Four pulses of intense fault block rotation (and hence fault motion) are indicated.

Fig. 9. Details of movement on high-angle reverse faults. Top left is a line-drawing interpretation of the shallow part of the MCS profile on the right. Displacements of a number of horizons at the two faults are given bottom left. These displacements were calculated using the velocity structure in the sedimentary cover established by Bull & Scrutton (1990b). The scatter in the value on the north fault probably arises in part from difficulty in interpretation near to the fault plane. The significance of the displacements is discussed in the text. Notice that within basement the south fault may displace and thus postdate the north fault.

Fig. 10. Log of cumulative frequency against, (a) log of amplitude (vertical throw of basement/cover interface) and (b) log of fault spacing, to test the power-law properties of the deformation.

Fig. 11. The top part shows the planform of deformation in a small area where track spacing is close enough to correlate individual faults along strike. Notice the angular relationships between the fracture zone, long wavelength undulation crest and reactivated, high-angle reverse faults (arrow head on hanging-wall side). Below, left is the theoretical angular relationship between the intraplate compressive stress direction ($\sigma_1$), the reactivated fracture zones and undulation crests and troughs. Below, right is the theoretical angular relationship between the reactivated fracture zones and the reactivated high-angle reverse faults, implying a component of dextral strike slip on the latter.

**Acknowledgements**

This work was supported by NERC grant GR3/6480. We thank the officers and crew of the RRS Charles Darwin and the technical support of R. V. S. Barry without whose expertise at seismic data collection this work would not have been possible. J. Cochran and J. Weissel kindly allowed access to the Lamont-Doherty Geological Observatory seismic profiles on which some of our ideas are based. Discussions with J. Andrews, M. Johnson, I. Main and J. Underhill were very useful.

**References**

BERGMAN, E. A. & SOLOMON, S. C. 1985. Earthquake source mechanisms from body wave inversion and intra-plate tectonics in the Northern Indian Ocean. Physics of the Earth and Planetary Interiors, 40, 1-23.

BULL, J. M. 1990. Structural style of intraplate deformation, Central Indian Ocean Basin: evidence for the role of fracture zones. Tectonophysics, 184, 213-228.

BULL, J.M. & SCRUTTON, R. A. 1990a. Fault reactivation in the Central Indian Ocean Basin and the rheology of the oceanic lithosphere. Nature, 344, 855-858.

BULL, J.M. & SCRUTTON, R. A. 1990b. Sediment velocities and deep structure from wide-angle reflection data around ODP Leg 116 sites. In: COCHRAN, J. R., STOW, D. A. - & - 19906. V. et al. Proceeding of the Ocean Drilling Program Scientific Results, 116: College Station Tx (Ocean Drilling Program).

BULL, J.M., MARTINOD, J. & DAVY, PH. 1992. Buckling of the Oceanic Lithosphere from Geophysical Data and Experiments. Tectonics, 11, 537-548.

CAMPBELL, A. C., PALMER, M. R. et al. 1988. Chemistry of hot springs on the Mid-Atlantic Ridge. Nature, 335, 514-519.

CHESTER, J. S. & CHESTER, F. M. 1990. Fault propagation folds above thrusts with constant dip. Journal of Structural Geology, 12, 903-910.

CLOETINGH, S. & WORTEL, R. 1986. Stress in the Indo-Australian plate. Tectonophysics, 132, 49-67.

CURRAY, J. R. & MOORE, D. G. 1974. Sedimentary and tectonic processes in the Bengal Deep-sea Fan and Geosyncline. In: BURK, C. A. & DRAKE, C. L. (eds) Continental Margins. Springer-Verlag, New York, 617-627.

CURRAY, J.R. & MUNASINGHE, T. 1989. Timing of intraplate deformation, northeastern Indian Ocean. Earth and Planetary Science Letters, 94, 71-77.

GELLER, G. A., WEISSEL, J. K. & ANDERSON, R. N. 1983. Heat transfer and intraplate deformation in the central Indian Ocean. Journal of Geophysical Research, 88, 1018-1032.

GORDAN, R. G., DEMETS, C. & ARGUS, D. F. 1990. Present day motion between the Australian and Indian plates: kinematic constraints on distributed lithospheric deformation in the Equatorial Indian Ocean. Tectonics, 9, 409-423.

HAXBY, W. F. & WEISSEL, 1. K. 1986. Evidence for small scale convection from SEASAT altimeter data. Journal of Geophysical Research, 91, 3507-3520.

HUANG, P. Y. & SOLOMON, S. C. 1988. Centroid depths of Mid-Ocean Ridge Earthquakes: dependance on spreading rate. Journal of Geophysical Research, 93, 13445-13477.

KOOPMAN, A., SPEKSNIJOER, A. & HORSFIELD, W.T. 1987. Sandbox model studies

LEGER, G. T. & LOUDEN, K. E. 1990. Seismic refraction measurements in the of inversion tectonics. Tectonophysics, 137, 379-388. Central Indian Basin: evidence for crustal thickening related to intraplate deformation. In: COCHRAN, J. R., STOW, D. A. V. et al. Proceedings of the Ocean Drilling Program. Ocean Drilling Program Scientific Reports, 116: College Station Tx.

LOWELL, J. D. 1970. Antithetic faults in upthrusting. American Association of Petroleum Geologists Bulletin, 54, 1946-1 950.

MACDONALD, K. C. & LUYENDYK, B. P. 1977. Deep-Tow Studies of the structure of the Mid- Atlantic crest near latitude 37" N. Geological Society of America Bulletin, 88, 621436.

MACDONALD, K. C. & LUYENDYK, B. P. 1985. Investigation of faulting and abyssal hill formation on the flanks of the East Pacific Rise (21"N). Marine Geophysical Researches, 7, 515-535.

MCADOO, D. C. & SANDWELL, D. T. 1985. Folding of the oceanic lithosphere. Journal of Geophysical Research, 90, 8563-8569.

MCCARTHY, J., MUTTER, J. C., MORTON, J. C., SLEEP, N. H. & THOMPSON, G. A. 1988. Relic magma chamber structures preserved within the Mesozoic North Atlantic crust? Geological Society of America Bulletin, 100, 1423-1436.

NEPROCHNOV, Y. P., LEVCHENKO, 0. V., MERKLIN, L. R. & SEDOV, V. V. 1988. The structure and tectonics of the intraplate deformation area in the Indian Ocean. Tectonophysics, 156, 89-106.

PETROY, D. E. & WIENS, D. A. 1989. Historical seismicity and implications for diffuse plate convergence in the northeast Indian Ocean. Journal of Geophysical Research, 94, 12301-12319.

PRUCHA, l. l., GRAHAM, 1. A. & NICHELSEN, R. P. 1965. Basement controlled deformation in Wyoming province of Rocky Mountains Foreland. American Association of Petroleum Geologists Bulletin, 49, 966-992.

RICHARD, P. & KRANTZ, R. W. 1991. Experiments on fault reactivation in strike-slip mode. Tectonophysics, 188, 117-131.

RIEDESAL, M., ORCUTT, J. A. MACDONALD, K. C. & MCCLAIN, J. S. 1982. Microearthquakes in the Black Smoker Hydrothermal Field, East Pacific Rise at 21"N. Journal of Geophysical Research, 87, 10613-10623.

ROYER, J. Y. & CHANG, T. 1991. Evidence for relative motions between the Indian and Australian plates during the last 20Myr from plate tectonic reconstructions. Implications for the deformation of the Indo-Australian plate. Journal of Geophysical Research, 96, 1 1 779-1 1 802.

ROYER, J. Y., PEIRCE, J. W. & WEISSEL, J.K. 1991. Tectonic constraints on the hot-spot formation of the Ninetyeast Ridge. In: WEISSEL, J. K., PEIRCE, J. W., TAYLOR, E., ALT, J. et al. Proceedings of the Ocean Drilling Program Scientific Results, 121, 763-776.

SHIPBOARD SCIENTIFIC PARTY 1989. ODP Leg l16 Site Survey. In: COCHRAN, I. R., STOW, D. A. V. et al. Proceedings of the Ocean Drilling Program Initial Reports, 116: College Station, Tx (Ocean. Drilling Program).

STEIN, C. A. & WEISSEL, J.K. 1990. Constraints on Central Indian Ocean Basin thermal structure from heat flow, seismicity and bathymetry Tectonophysics, 176, 315-332.

STEIN, C.A., CLOETINGH, S. & WORTEL, R. 1989. Seasat-derived gravity constraints on stress and deformation in the north-eastern Indian Ocean. Geophysical Research Letters, 16, 823-826.

SYKES, L. R. 1970. Seismicity of the Indian Ocean and a possible nascent island arc between Ceylon and Australia. Journal of Geophysical Research, 75, 5041-5055.

WALSH, J., WATTERSON, I. & YIELDING, G. 1991. The importance of small-scale faulting in regional extension. Nature, 351, 391-393.

WEISSEL, J. K. & GELLER, C. A. 1981. Preliminary results of 1980 shipboard investigations of deformation of the Indo-Australian plate. I-Seismic Reflection. EOS Transactions of the American Geophysical Union, 62, 404.

WEISSEL, J.K. & HAXBY, W. F. 1984. A tectonic tour of the Indian Ocean via the SEASAT satellite. EOS Transactions of the American Geophysical Union, 65, 185.

WEISSEL, J.K., ANDERSON, R. N. & GELLER, C. A. 1980. Deformation of the Indo-Australian plate. Nature, 287, 284-291.

WHITE, R. S., DETRICK, R. S., MUTTER, J. C., BUHL, P, MINSHULL, T. A. & MORRIS, E. 1990. New seismic images of oceanic crustal structure. Geology, 18, 462-465.

WILLIAMS, C. F. 1990. Hydrothermal circulation and intraplate deformation: constraints and predictions from in-situ measurements and mathematical models. In: COCHRAN, J. R., STOW, D. A. V. et al. Proceedings of the Ocean Drilling Program Scientific Reports, 116: College Station Tx (Ocean Drilling Program).

ZUBER, M. T. 1987. Compression of the oceanic lithosphere: an analysis of intraplate deformation in the Central Indian Basin. Journal of Geophysical Research 92, 4817-4825.

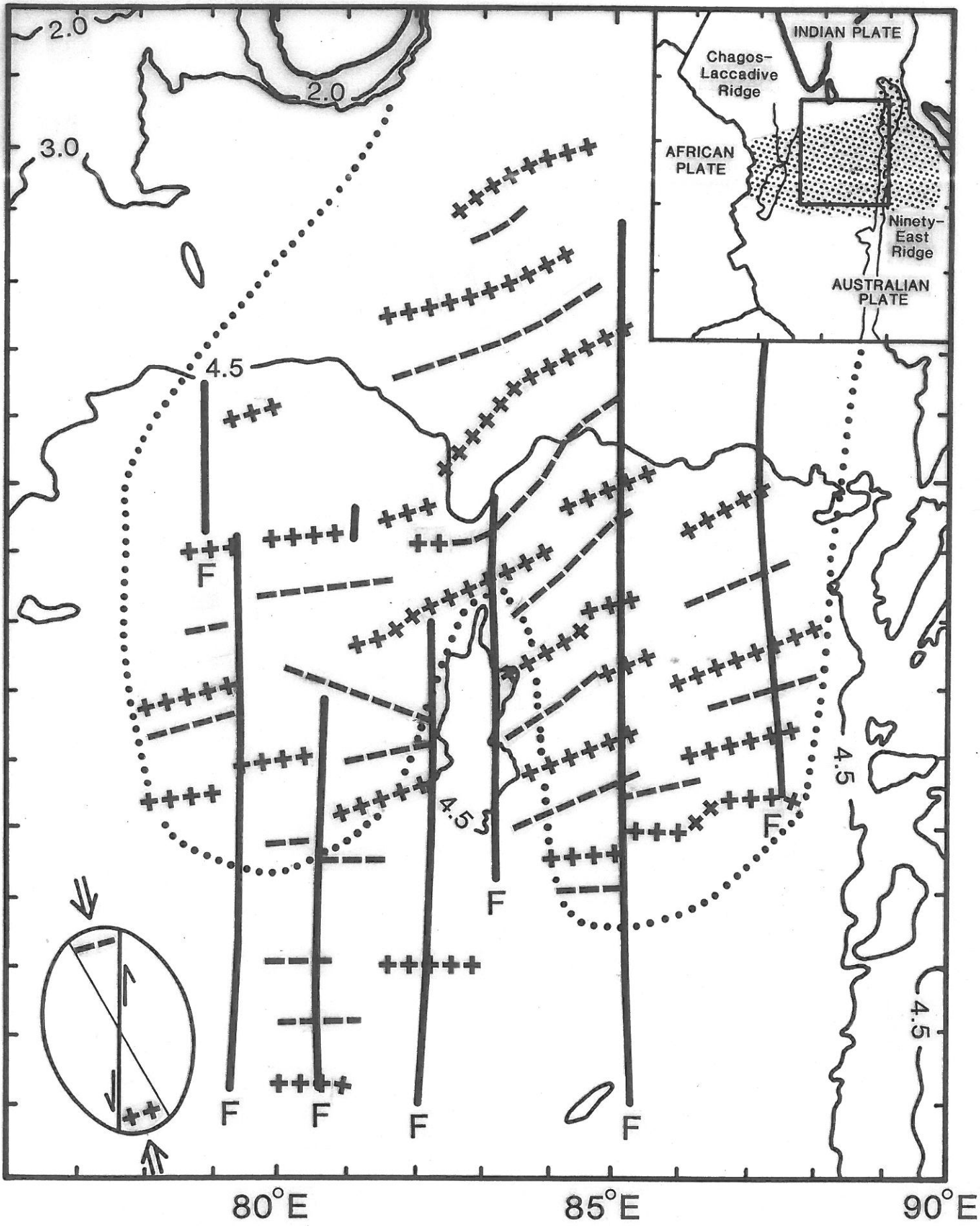


91/121
Fig 1
40%.

Bull & Scrutton Fig 1 40%

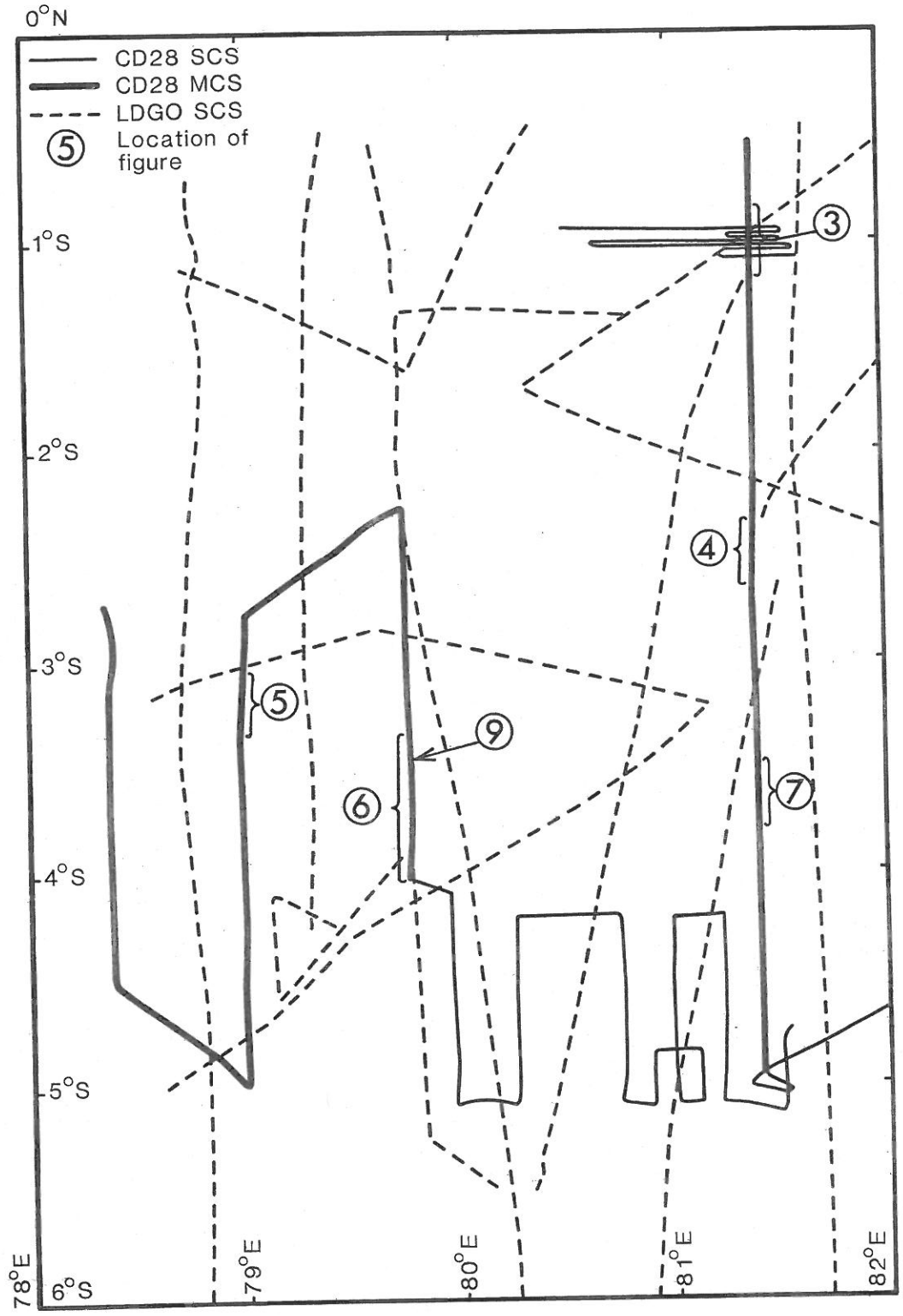


91/131
Fig 2
43%

Fig 2

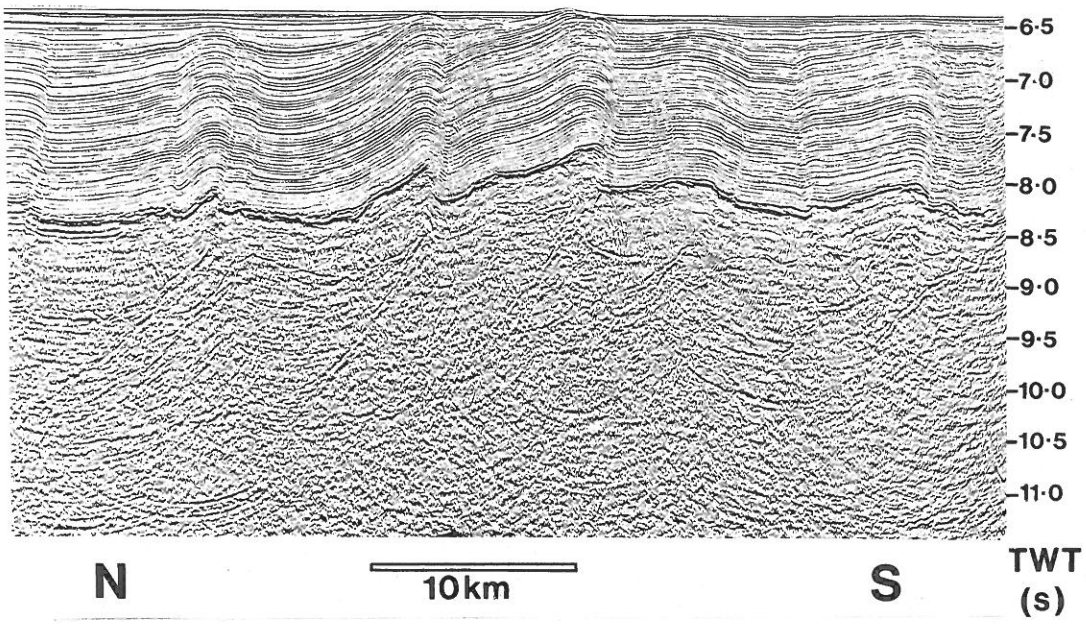


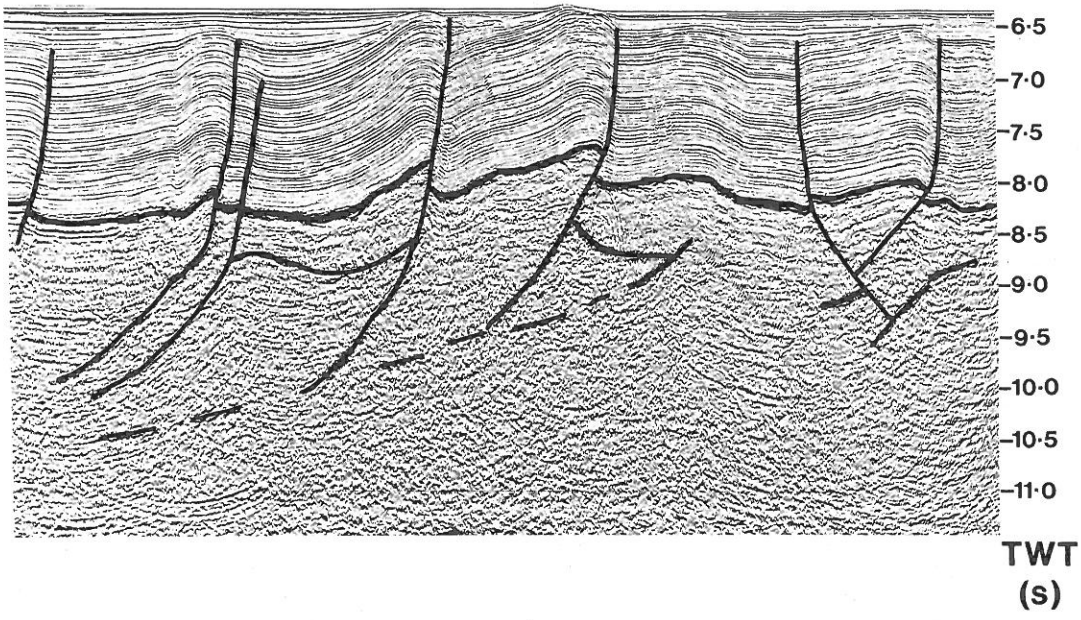


91/131
Fig 3
60%

3

JGS 91/131 Fig. 3. Bull & Scrutton 60%

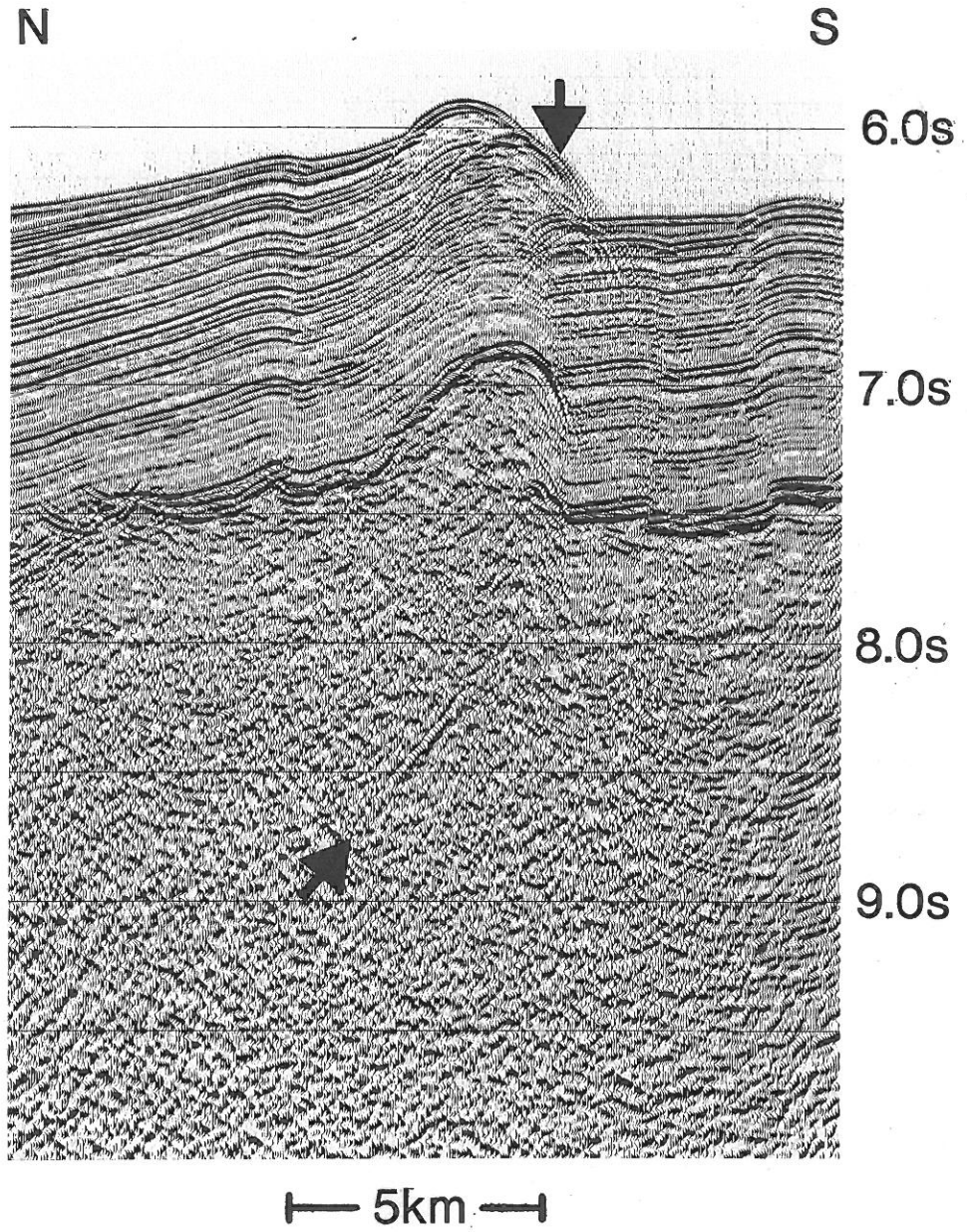


91/131
Fig 4
68%

68%
JGS 91/131 Bull & Scrutton Fig. 4

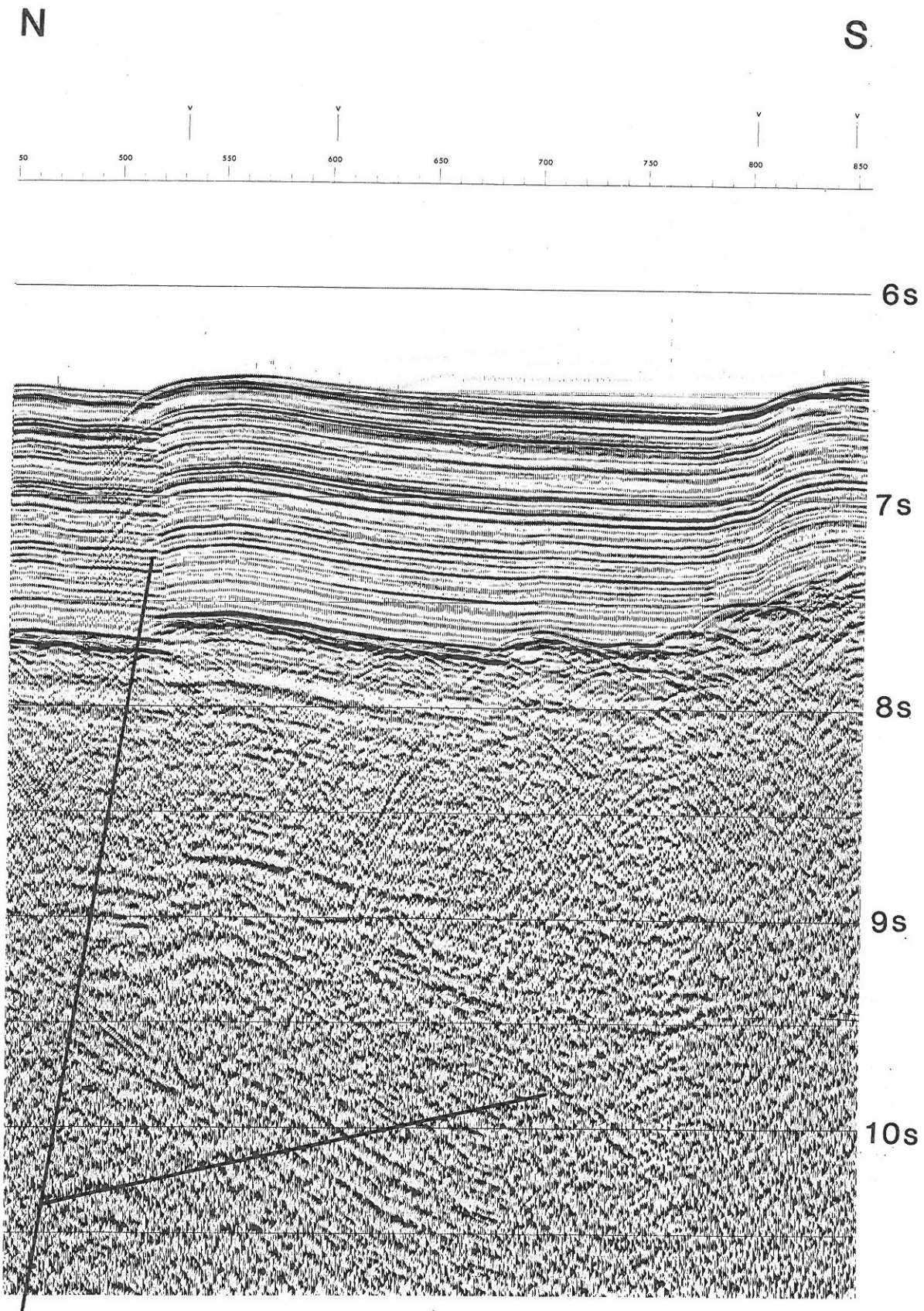
N
S
50
500
550
600
650
700
750
800
850
6s
7s
8s
9s
10s
5 km
Southward dipping reverse
fault in basement and overlying cover

Figure 5.

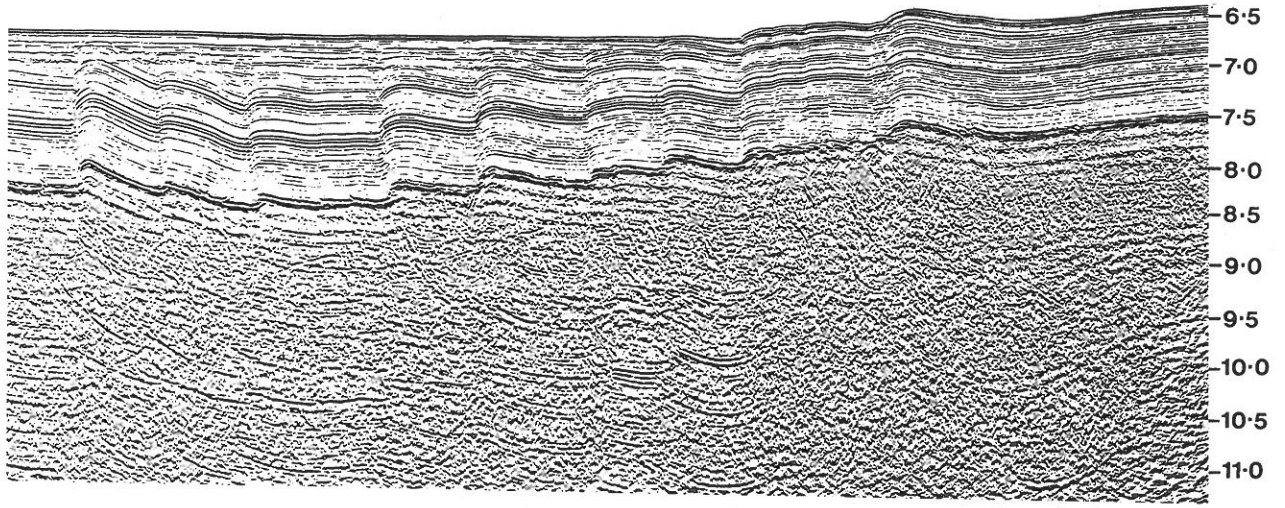


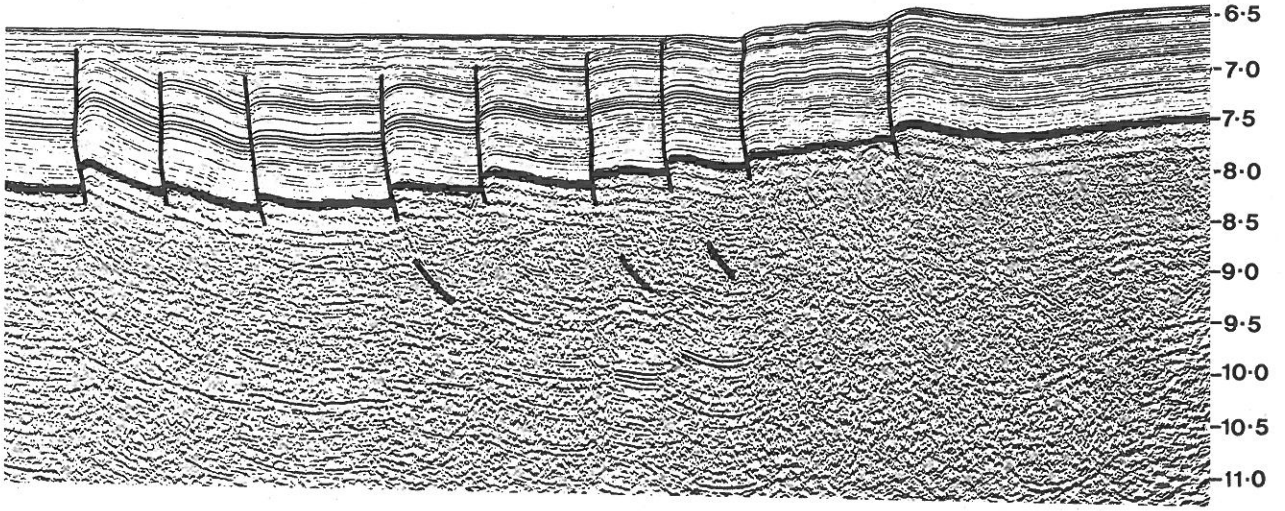


JGS 91/131
Bull. Scottish
Fig 6
60%

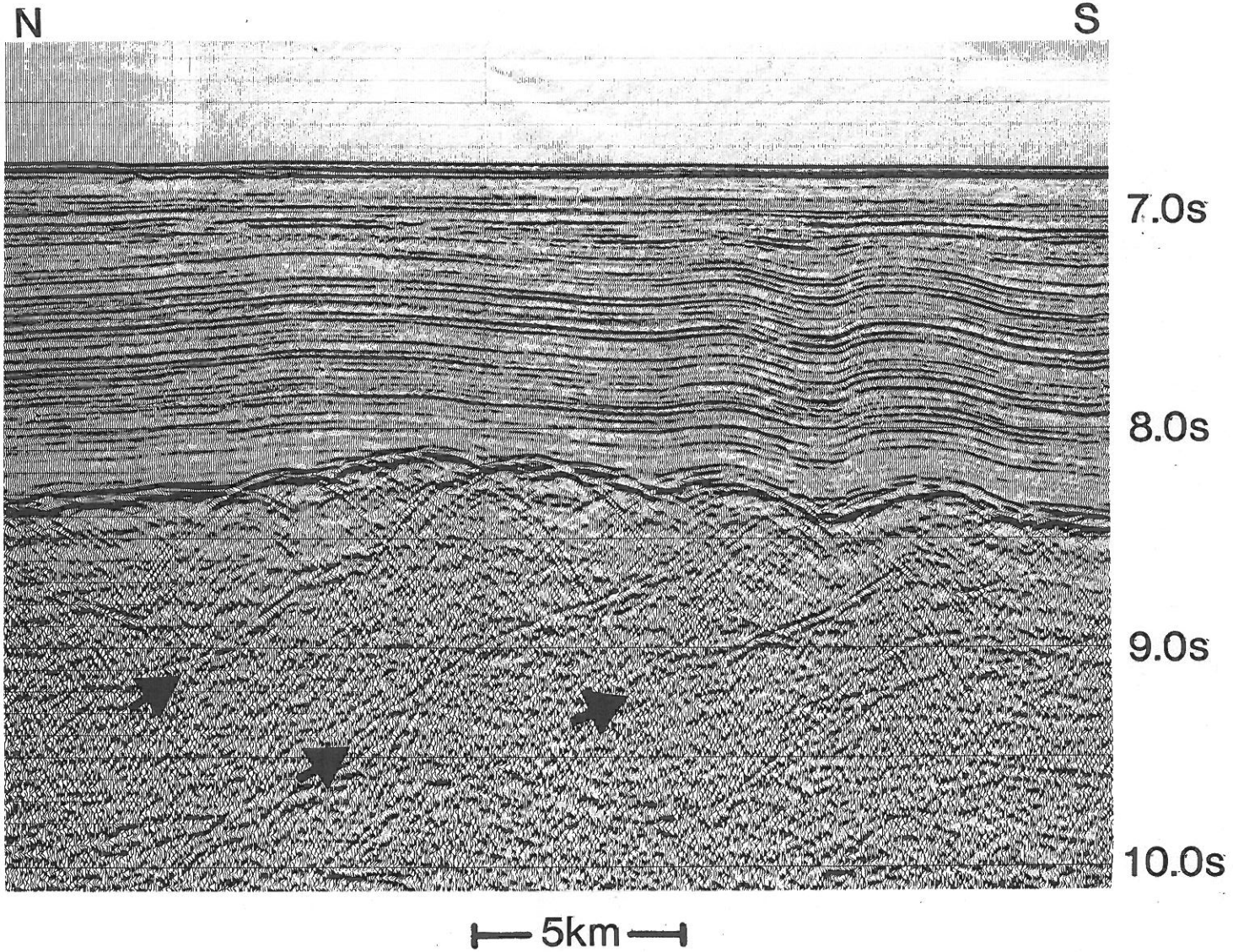


91/131
Fig 7
68%

68%
Tr 91/131 Bull & Scrutton fig 7

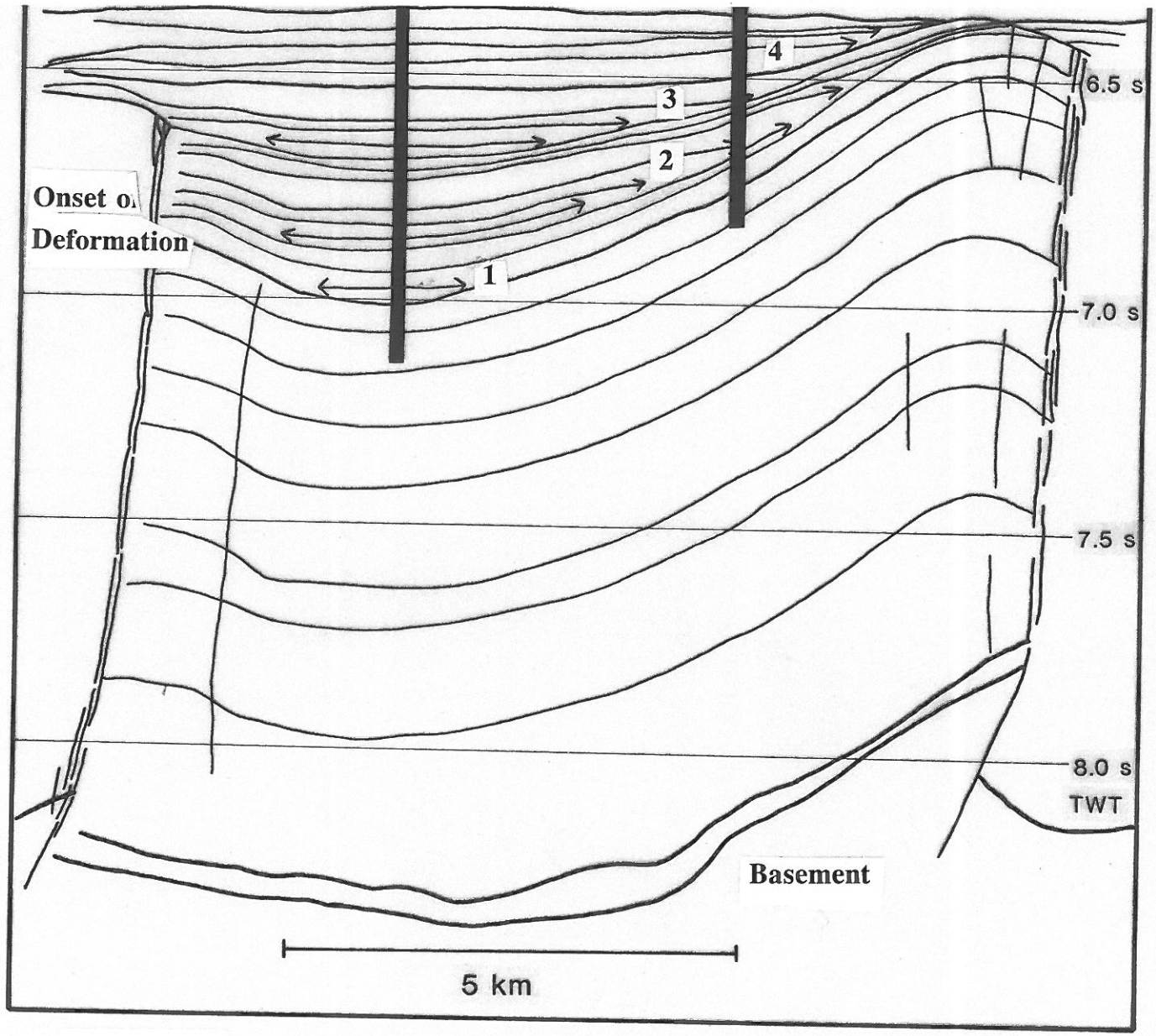


91/131
Fig 8
34%

JGS 91/131 Bull & Scrutton Fig 8 34%

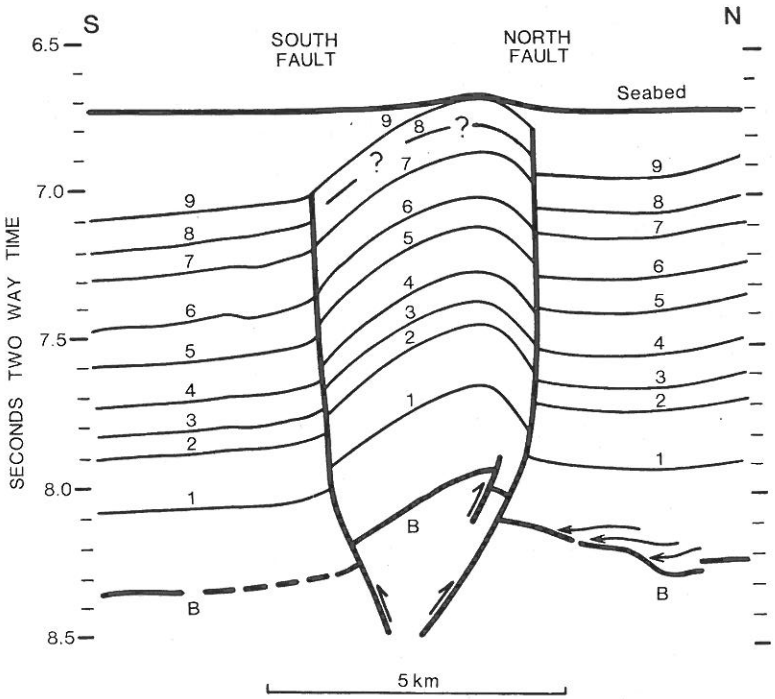


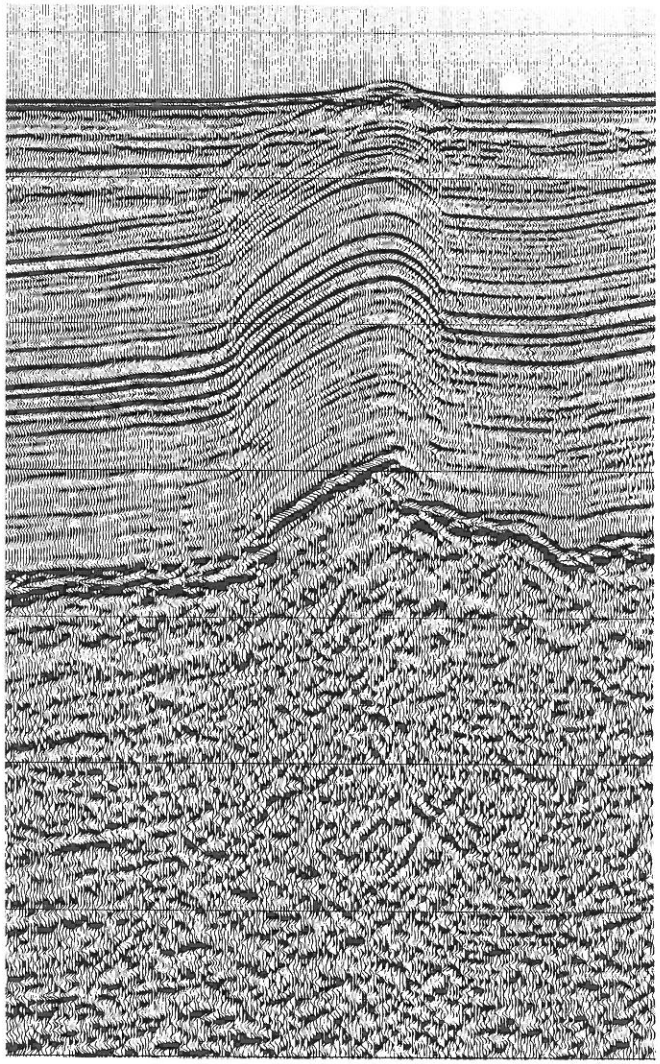

| HORIZON NUMBER | SOUTH FAULT DISPLACEMENT | NORTH FAULT DISPLACEMENT |
|---|---|---|
| 9 | <18m | ?150m |
| 8 | <18m | 200m |
| 7 | <18m | 199m |
| 6 | 18m | 178m |
| 5 | 50m | 172m |
| 4 | 54m | 156m |
| 3 | 76m | 170m |
| 2 | 80m | 150m |
| 1 | 107m | 124m |
| B | 134m | 151m |

91/131
Fig 9
68%

JGS 91/131 Bull & Scrutton fig 10a 70%
Please add (a)

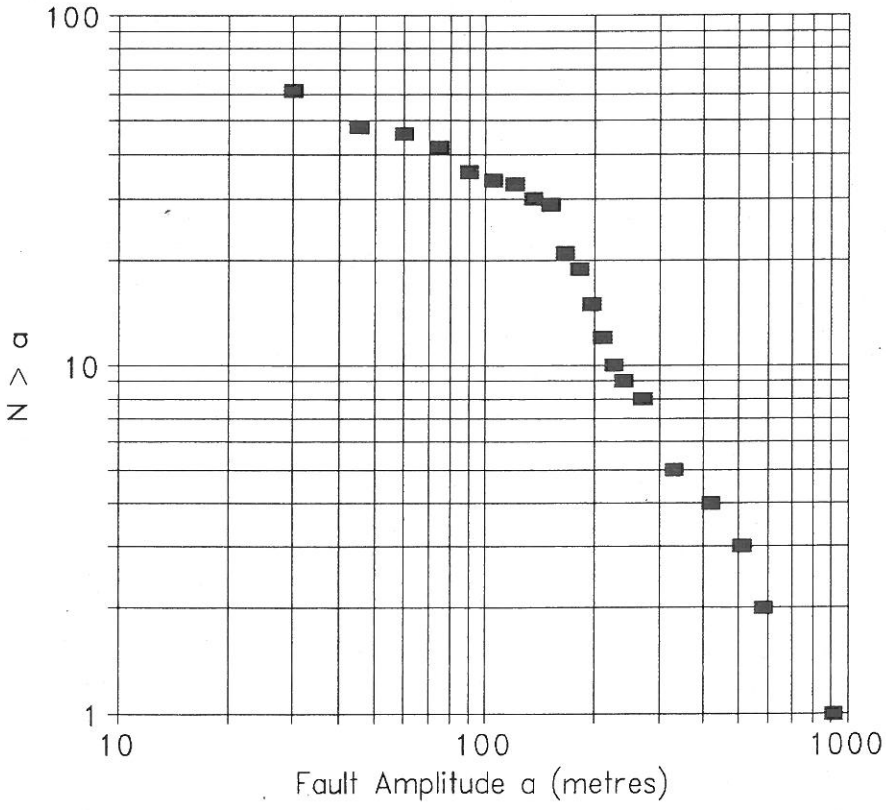


91/131
Fig 10A
70%

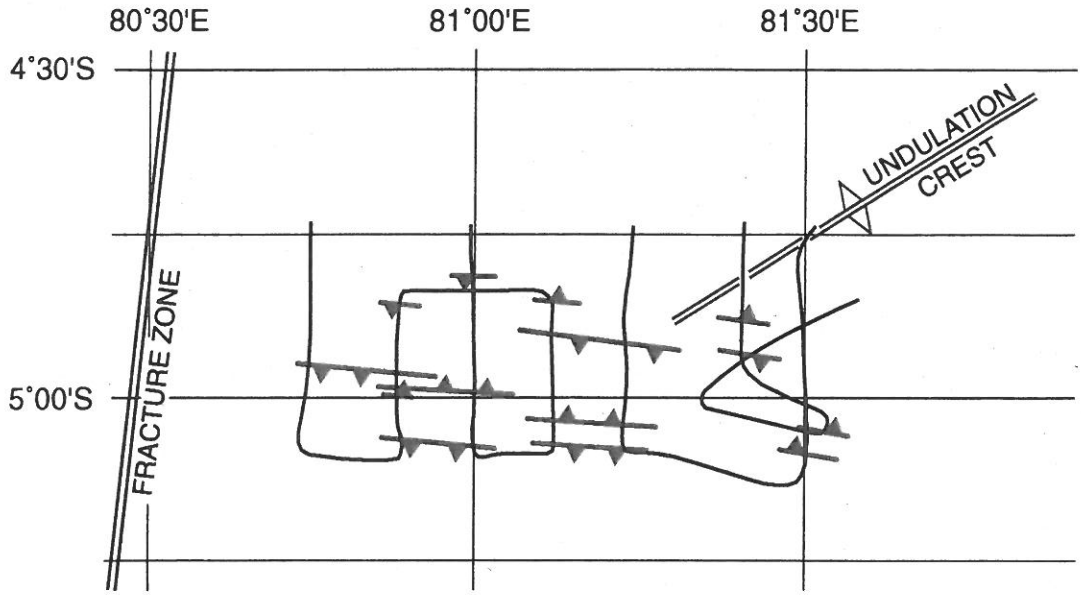
80°30'E
81°00'E
81°30'E
4°30'S
5°00'S
FRACTURE ZONE
UNDULATION
CREST

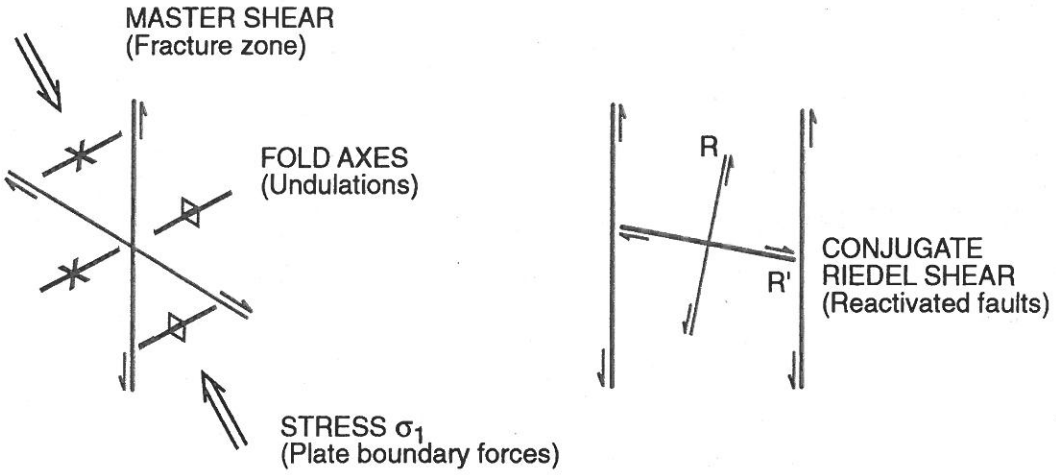
MASTER SHEAR
(Fracture zone)
FOLD AXES
(Undulations)
STRESS $\sigma_1$
(Plate boundary forces)
R
R'
CONJUGATE
RIEDEL SHEAR
(Reactivated faults)

Fig 11.